PHYSICAL REVIEW B **94**, 180102(R) (2016)

Effects of atomic short-range order on properties of the $PbMg_{1/3}Nb_{2/3}O_3$ relaxor ferroelectric

Sergey Prosandeev[1,2] and L. Bellaiche[1]

[1]*Physics Department and Institute for Nanoscience and Engineering, University of Arkansas, Fayetteville, Arkansas 72701, USA*

[2]*Institute of Physics and Physics Department of Southern Federal University, Rostov-na-Donu 344090, Russia*

(Received 12 September 2016; published 3 November 2016)

The effect of atomic *short-range* order on the macroscopic and microscopic properties of the prototype of relaxor ferroelectrics, that is, lead magnesium niobate $Pb(Mg_{1/3}Nb_{2/3})O_3$ (PMN), is studied via the combination of an annealing technique and a large-scale effective Hamiltonian method. The investigated short-range order gradually varies from the case of fully disordered solid solutions to the situation for which the first three nearest-neighboring shells of the B lattice of PMN adopt a rocksalt ordering between a sublattice made of pure Nb ions and a randomly distributed sublattice consisting of $\frac{2}{3}$ of Mg and $\frac{1}{3}$ of Nb. The characteristic temperatures of relaxor ferroelectrics (namely, the Burns, so-called T^*, and depolarizing temperatures) significantly increase when strengthening this short-range chemical order, which is accompanied by an overall enhancement of the size of the polar nanoregions as well as of some antiferroelectric interactions. These results can be understood by the fact that chemical short-range order strongly modifies the internal electric fields felt by the Pb ions.

DOI: 10.1103/PhysRevB.94.180102

Relaxor ferroelectrics form an important class of disordered materials that are characterized by large and strongly frequency-dependent dielectric permittivity as well as by several unusual characteristic temperatures [1,2], with these compounds remaining macroscopically paraelectric down to 0 K. One of these characteristic temperatures is the famous Burns temperature [3], at which it is commonly believed that relaxor ferroelectrics begin to acquire polar nanoregions that are responsible for their anomalous properties. Another temperature is often denoted as T^* and is associated with an anomaly in acoustic emission and in the temperature dependence of the lattice constant, with striking features in the Raman and neutron scatterings [4–9]. A third characteristic temperature is the depolarizing temperature, at which the poled relaxor system loses its polarization on heating [10–13]. Relaxor ferroelectrics continue to attract attention in order to fully understand their unusual properties, as, e.g., demonstrated by recent computational studies shedding new light onto them (see, e.g., Refs. [14–19] and references therein).

It is also important to realize that the theory of (classical) ferroelectrics typically considers long-range electrostatic interactions as the main cause of ferroelectricity [20], and that such latter interactions can be modified in relaxors by, e.g., the simultaneous presence of both ferroelectrically active and inactive ions inside these systems [21,22] or by the existence of so-called random electric fields [10] or random strains originating from the difference in charge and size, respectively, of the mixed ions. As a result, one may dramatically alter the characteristic temperatures of relaxor ferroelectrics if one can vary these random fields. One way to change them is to modify the *long-range* chemical ordering between the mixed ions, as experimentally found (by changing the growth conditions) and theoretically predicted in, e.g., Refs. [23,24] for $PbSc_{1/2}Ta_{1/2}O_3$ and $PbSc_{1/2}Nb_{1/2}O_3$ systems, when going from disordered to long-range rocksalt-ordered structure.

However, several relaxor ferroelectrics, including the prototype lead magnesium niobate $Pb(Mg_{1/3}Nb_{2/3})O_3$ (PMN), do not present a long-range ordering between the mixed ions but rather possess a chemical order of short-range nature, as, e.g., evidenced by the small intensity of x-ray superstructure peaks found in Refs. [25,26]. Strikingly, the effect of chemical short-range order on the properties of relaxor ferroelectrics is not well known. For instance, it is not clear if and how short-range chemical order can affect the macroscopic and local properties of relaxor ferroelectrics, and if the (hypothetical) variation of these quantities can be understood at a microscopic level. One reason for this paucity of knowledge is that it is difficult to experimentally extract the amount (and type) of short-range order present in a relaxor ferroelectric. Another reason is that simulating short-range order is not a straightforward task since one needs to mimic very specific short-range atomic correlations, which also requires the use of large supercells.

The aims of this Rapid Communication are to provide the answers to these issues, by combining an annealing technique and an effective Hamiltonian scheme, and to reveal that not only many properties of PMN strongly depend on chemical short-range order but also that these dependencies are linked to the internal electric fields felt by the Pb ions.

Here, the effect of short-range order on the properties of PMN is investigated by first considering $18 \times 18 \times 18$ supercells made of virtual $Pb(Nb_{0.5}\langle B_{av}\rangle_{0.5})O_3$ solid solutions, where $\langle B_{av}\rangle$ is an artificial atom made of $\frac{2}{3}$ of Mg and $\frac{1}{3}$ of Nb. The chemical ordering of this $Pb(Nb_{0.5}\langle B_{av}\rangle_{0.5})O_3$ system is then introduced via the concept of Cowley parameters [27–30] that are defined as

$$\alpha_j = 1 - 2P_j, \tag{1}$$

where P_j is the probability of finding a Nb (respectively, $\langle B_{av}\rangle$) atom being the jth nearest neighbor of a $\langle B_{av}\rangle$ (respectively, Nb) atom in the mixed B sublattice. Here, we practically consider $j = 1$, 2, and 3 (that is, the first, second, and third nearest neighbors' shells of the B sublattice) and impose $\alpha_1 = -\alpha$, $\alpha_2 = +\alpha$, and $\alpha_3 = -\alpha$, with α varying between $+0.0$ (which characterizes perfect disorder between the Nb and $\langle B_{av}\rangle$ ions) and $+1.0$ (which corresponds to rocksalt ordering of the first three neighboring shells between the Nb and $\langle B_{av}\rangle$ ions) by steps of 0.1. Such a procedure is technically performed via an annealing method [30] aiming to reach the desired values of α_1, α_2, and α_3, and therefore leads to the generation of 11 different supercells, each associated with

its own α and thus representative of different short-range chemical orderings (note that we numerically found that imposing $\alpha_1 = -1$, $\alpha_2 = +1$, and $\alpha_3 = -1$ results in fact in the long-range atomic ordering of a rocksalt type of *all* the shells, that is, the corresponding configuration adopts long-range rocksalt ordering in addition to short-range rocksalt ordering; note also that we did not consider here the existence of rocksalt-ordered regions existing inside a disordered matrix as in Refs. [16,17]). For each of these 11 supercells, we then use a *random* number generator to replace the virtual $\langle B_{\rm av}\rangle$ atoms by real Mg and Nb ions in 2 : 1 proportion. Note that we practically use 30 different random numbers, which effectively results in the generation of 30 different configurations for any considered α. The properties of these 30 configurations are then averaged in order to better mimic the disorder inherent in the $\langle B_{\rm av}\rangle$ sublattice (note that such a procedure for $\alpha = +1$ is consistent with the so-called "random site" model of PMN [25,26] that is characteristic of a 1:1 chemical order, inside which pure Nb planes alternate along the [111] pseudocubic direction with planes containing a random mixture of $\frac{1}{3}$ of Nb and $\frac{2}{3}$ of Mg ions).

The atomistic effective Hamiltonian of Ref. [31] is then employed to model the effect of these chemical orders on the properties of PMN by using all the aforementioned constructed supercells within Monte Carlo simulations. Its degrees of freedom are (1) the local modes $\mathbf{u_i}$ at each five-atom unit cell i and that are centered on Pb ions (these local modes are directly proportional to local electric dipoles), and (2) the homogeneous and inhomogeneous strains. More details about this effective Hamiltonian are given in the Supplemental Material [31–34].

Figure 1(a) shows the predicted averaged diagonal component of the dielectric tensor χ (i.e., $\frac{1}{3}$ of the trace of this tensor) as a function of temperature for the investigated short-range order parameters. Such a dielectric response adopts a broad peak for any considered α, as is characteristic of relaxor ferroelectrics [1,2]. This broad peak is centered around a temperature that depends on the amount of short-range ordering, that is, about 350–400 K for $\alpha = 0$ versus about 500 K for $\alpha = 1$. Results obtained in Ref. [24] for another relaxor ferroelectric, $Pb(Sc_{0.5}Nb_{0.5})O_3$, showing that the diffuse peak of dielectric permittivity shifts to higher temperatures when going from a disordered system to a chemically rocksalt-ordered compound, are therefore also valid for PMN. It is interesting to realize that Ref. [26] also observed that the position and intensity of the dielectric permittivity peak in PMN:Tb change after thermal annealing at high temperatures, as a result of the emergence of large rocksalt-ordered domains. Note that, as is also characteristic of relaxor ferroelectrics [1,2], PMN is found to be paraelectric down to the lowest investigated temperatures for any studied α, except for a few configurations that can have nonvanishing polarization below $\simeq$300 K, especially for larger α. For example, at $\alpha = 1$ and $T = 50$ K, there are three configurations with significant polarization among the 30 investigated supercells. On the other hand, the magnitude of the local mode, as averaged over the 30 configurations, is rather small for any α. In other words, PMN can be thought to be paraelectric on average, independently of our studied short-range chemical ordering. Note that the few configurations that exhibit a significant polarization are responsible for the enhancements of the dielectric response (for which values are above $\simeq$2000) seen in Fig. 1(a) for temperatures below 300 K. Such (anomalous) enhancements indicate that the relaxor and ferroelectric phases are close to each other in energy in PMN, and that the atomic distribution between Nb and Mg ions can alter their energetics. Moreover, Fig. 1(b) reports the *inverse* of χ as a function of temperature. This function can be well fitted by a straight line for temperatures higher than the Burns temperature [3] (to be denoted as T_B in the following), with the interpolation of this straight line with the zero occurring at a temperature that we estimate to be the T^* characteristic temperature of relaxor ferroelectrics [4–9]. Figure 1(c) reveals the rather strong dependency of T^* on α. For instance, T^* increases from about 397 to $\simeq$508 K when α varies from 0 to 1. For comparison, different experiments indicated a T^* being close to 350 K in Ref. [6], near 400 K in Refs. [4,5,8], and as high as 500 K in Ref. [7]. This observed large variation can therefore be explained by a difference in atomic short-range ordering according to our simulations. Figure 1(c) further indicates that our computed T_B are less sensitive to α than T^*: It is about 605 K at $\alpha = 0$ and 660 K at $\alpha = 1$, that is, T_B varies by only 9% while T^* is enhanced by about 28% when α increases from 0 to 1. Note that our predicted range for T_B also includes the Burns temperature of 620 K reported in Ref. [3] for PMN.

Let us now determine if short-range ordering in PMN has some effect on the microstructure. For that, in the insets of Fig. 2(a) we report snapshots of the electric dipolar pattern for a single configuration of two different α parameters, namely, $\alpha = 0$ and 1, at 50 K. In these insets, the red lines delimit polar nanoregions (PNRs) inside which the dipoles are nearly parallel to each other, and existing within our $18 \times 18 \times 18$ supercells. These PNRs are determined using the same method as in Ref. [35] and their size is estimated [36] as $s = \langle N_{\rm PNR}^2\rangle/\langle N_{\rm PNR}\rangle$, where $N_{\rm PNR}$ is the number of the sites belonging to a particular polar nanoregion while $< >$ denotes averages over the different PNRs. Figure 2(a) reports the dependency of s with α (as averaged over the 30 investigated configurations for each α), which reveals that polar nanoregions typically grow in size if one increases the degree of the chemical short-range order—as consistent with the comparison between the left and right insets of this figure. This cluster size nearly doubles on average from 13 to 24 sites when going from the disordered case to the atomic arrangements corresponding to $\alpha = +1$. We also found the Edwards-Anderson parameter (see Ref. [22] and references therein for the definition of this parameter) to increase its magnitude when decreasing temperature for all studied values of α.

Moreover, various studies suggested that antiferroelectricity (AFE) also plays some role in relaxor ferroelectrics [31,37–39]. To check such a fact and determine how such AFE depends on short-range chemical order in PMN, we computed the magnitudes of the Fourier transform [40] of the x components of the local modes in the considered supercells [41]. The largest Fourier transforms correspond to the following q points [42], $2\pi(n_x,n_y,n_z)/18a_{\rm lat}$, where $a_{\rm lat}$ is the five-atom cubic lattice constant and with $(n_x,n_y,nz) =$ (2,0,−2), (−2,0,2), (−2,2,0), (2,−2,0), (−2,−2,0), (2,2,0), (2,0,2), and (−2,0,−2). Figure 2(b) reports the dependence of the sum of the magnitudes of these eight largest Fourier

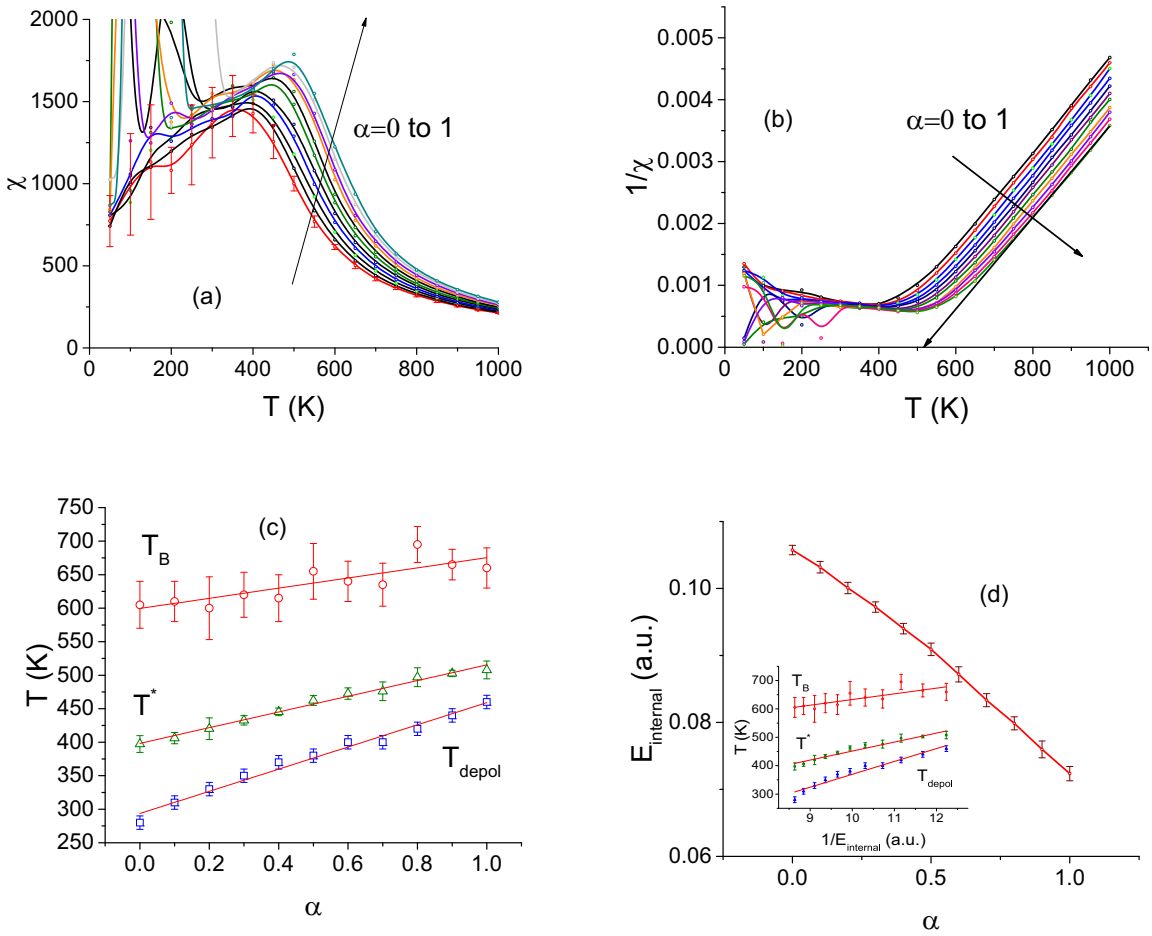

FIG. 1. Predicted properties of PMN as a function of the chemical short-range order parameter α: (a) dielectric permittivity; (b) inverse of the dielectric permittivity; (c) the T_B, T^*, and T_{depol} characteristic temperatures (see text); and (d) the averaged magnitude of the internal electric field E_{internal} acting on Pb ions. The inset in (d) presents the dependence of T_B, T^*, and T_{depol} on the inverse of E_{internal}. The solid lines are guides for the eyes, and error bars result from the summation over 30 different configurations for each α.

transforms on α at 50 K, which demonstrates that short-range order has the tendency to also enhance antiferroelectric correlations—in addition to strengthening the size of the PNRs on average [as shown in Fig. 2(a)]. Interestingly, these AFE correlations are not negligible, once realizing that the sum of the magnitudes of the Fourier transforms [40] of the x components of the local modes on *all* q points amounts to unity and that the data reported in Fig. 2(b) vary between $\simeq$0.38 and $\simeq$0.53. Note also that both Figs. 2(a) and 2(b) indicate that this sum as well as the size of the PNRs also strongly depend on the different configurations used for any given α, as demonstrated by the large error bars provided in these figures, which further demonstrates the significant effect of the atomic distribution of Mg and Nb ions on the properties of PMN.

In order to have a real-space picture of correlations between electric dipoles, we also computed

$$\theta_{x,x}(\mathbf{r}) = \frac{1}{N_{\text{Pb}}} \sum_i \frac{u_{i,x} u_{i+r,x}}{|\mathbf{u_i}||\mathbf{u_{i+r}}|}, \tag{2}$$

where the sum runs over all the N_{Pb} Pb sites i of the system. $\mathbf{u_i}$ and $\mathbf{u_{i+r}}$ are the local modes in cell i and in the cell centered on the Pb atom distant by $\mathbf{r}$ from cell i, respectively, and $u_{i,x}$ and $u_{i+r,x}$ are their x components, respectively. The two insets of Fig. 2(b) display $\theta_{x,x}(\mathbf{r})$ as averaged over the (001) planes, for the same configurations used for the insets of Fig. 2(a), for $\alpha = 0$ and 1. These two insets both show (i) ferroelectric correlations [for which $\theta_{x,x}(\mathbf{r})$ is positive] for distances less than $2a_{\text{lat}}$ in the (x, y) plane, as consistent with the existence of the (small) polar nanoregions depicted in the insets of Fig. 2(a), and (ii) strong antiferroelectric correlations [for which $\theta_{x,x}(\mathbf{r})$ is negative and with a magnitude of about 0.13 for $\alpha = 0$ and 0.18 for $\alpha = 1$] at, e.g., distances of $4a_{\text{lat}}$ and $5a_{\text{lat}}$ along the x axis as well as those deduced from them by translation along the y axis by $9a_{\text{lat}}$. Such AFE is in line with the significant sum of the Fourier transforms of Fig. 2(b) and with the predictions of the importance of the antiferroelectric interactions on the relaxor properties [37].

We also conducted simulations corresponding to zero field heating (ZFH) after (i) field cooling (FC) PMN down to 50 K under an electric field of $\sqrt{3} \times 10^8$ V/m magnitude and oriented along the [111] direction and (ii) then removing such a field before heating the system. As consistent with known features of PMN [10–13], such a procedure leads to the formation of a polarization along the [111] direction that we denote here as $P_{\text{ZFH-FC}}$. Such a polarization exists from low

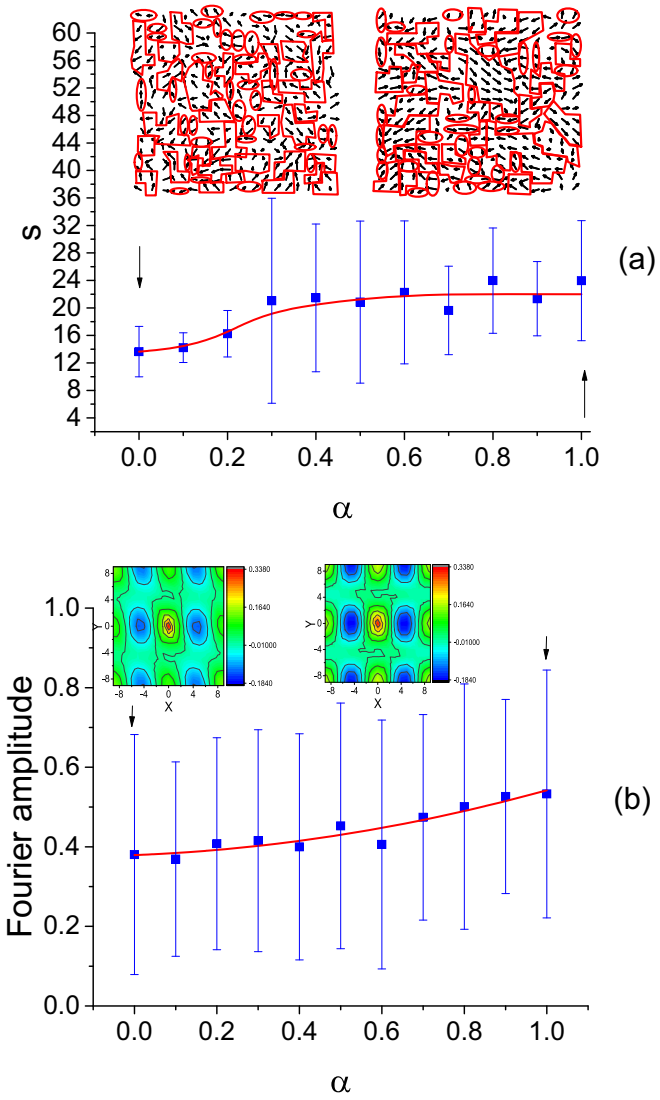

FIG. 2. Computed microscopic properties of PMN as a function of the chemical short-range order parameter α, at 50 K: (a) average size s of the polar nanoregions (see text) and (b) sum (over the eight specific q points indicated in the text) of the magnitudes of the Fourier transform of the x components of the local modes. The left and right insets of (a) are snapshots of the local modes' pattern for a single configuration corresponding to $\alpha = 0$ and 1, respectively, with the polar regions being delimited in red. The left and right insets of (b) report the $\theta_{x,x}$ quantity [see Eq. (2)] as averaged over the (001) planes of these two latter configurations, respectively. The solid lines are guides for the eyes, and error bars result from the summation over 30 different configurations for each α.

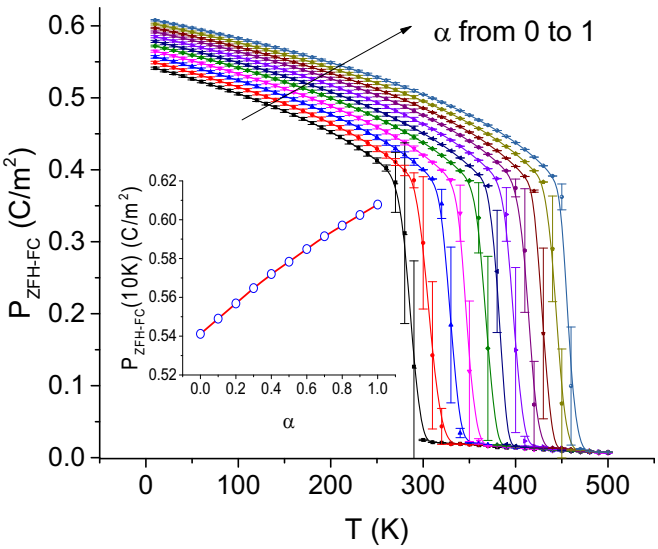

FIG. 3. Temperature dependence of the $P_{\text{ZFH-FC}}$ polarization (see text) for the different investigated α parameters. The inset shows the magnitude of this polarization calculated at 10 K, as a function of α. Error bars result from the summation over 30 different configurations for each α.

temperatures up to a specific temperature, which is typically coined the depolarizing temperature [10–13] and that we will refer to as T_{depol}, above which the systems suddenly revert to its relaxor state (for which the macroscopic polarization is null). Figure 3 shows the behavior of $P_{\text{ZFH-FC}}$ versus temperature for different α which, e.g., allows us to extract the dependency of two different quantities on short-range order: (i) T_{depol}, which is displayed in Fig. 1(c) (along with T^* and T_B), and (ii) $P_{\text{ZFH-FC}}$ calculated at our lowest investigated temperature of 10 K, which is reported in the inset of Fig. 3. Both T_{depol} and $P_{\text{ZFH-FC}}$ at 10 K increase with α, which indicates that short-range order clustering has the tendency to deepen the energy well of the ferroelectric phase in addition to moving it to a larger polarization at low temperature. Note that T_{depol} in our calculations changes from 280 ± 10 K at $\alpha = 0$ to 459 ± 10 K at $\alpha = 1$, while data of about 210 K were reported in Ref. [11].

With the aim to understand the origin of the aforementioned striking dependency of the macroscopic and local properties of PMN on the degree of the chemical order, we further calculated the internal electric field $\mathcal{E}_{\mathbf{i}}$ felt by each Pb ion (and due to the difference in charges between Nb and Mg ions) in our $18 \times 18 \times 18$ supercells (see the Supplemental Material and Refs. [16,31,33,43,44] for details about this calculation). An averaged magnitude of internal electric fields is then defined as $E_{\text{internal}} = \sqrt{\frac{1}{N_{Pb}} \sum_i |\mathcal{E}_{\mathbf{i}}|^2}$. Figure 1(d) shows such a magnitude and reveals that E_{internal} decreases as α increases. As shown in the inset of Fig. 1(d), this decrease is linearly correlated (and thus explains) the concomitant enhancement of the T^*, T_B, and T_{depol} temperatures with α. One can thus safely conclude that the properties of PMN are strongly linked to their internal electric fields, as consistent with Refs. [10,16,31,45]. In particular, Ref. [31] predicted that the full (but unpractical) annihilation of internal electric fields inside PMN would result in a ferroelectric ground state, which is consistent with the fact that T_{depol} is the highest, and also the closest to T^*, when $\alpha = 1$ in all our investigated short-range ordered configurations.

In summary, we demonstrated that chemical short-range order can highly affect the macroscopic properties of PMN, such as the diffuse dielectric permittivity peak position, the polarization in its field-induced ferroelectric phase, as well as the Burns, T^*, and depolarizing temperatures. Such ordering has also an overall effect on microscopic quantities, such as the size of the polar nanoregions and antiferroelectric interactions. These effects originate from the fact that varying

the chemical short-range order is one effective way to alter the internal electric fields felt by the Pb ions. We therefore hope that this Rapid Communication helps in better understanding complex solid solutions in general, and relaxor ferroelectrics in particular. It can also motivate the study of chemical short-range order on properties not studied here, such as dielectric relaxation [18].

This work is financially supported by ONR Grant No. N00014-12-1-1034 and ARO Grant No. W911NF-16-1-0227. S.P. also appreciates the Russian Foundation for Basic Research (Grant No. 16-52-00072 Bel_a). The computations were made possible thanks to the MRI Grant 0722625 from NSF, the ONR Grant No. N00014-15-1-2881 (DURIP) and a Challenge grant from the Department of Defense.

[1] L. E. Cross, Ferroelectrics **151**, 305 (1994).
[2] G. A. Smolensky *et al.*, *Ferroelectrics and Related Materials* (Gordon and Breach, New York, 1981).
[3] G. Burns and F. H. Dacol, Phys. Rev. B **28**, 2527 (1983); Solid State Commun. **48**, 853 (1983).
[4] D. Viehland, S. J. Jang, L. E. Cross, and M. Wuttig, Phys. Rev. B **46**, 8003 (1992).
[5] B. Dkhil, J. M. Kiat, G. Calvarin, G. Baldinozzi, S. B. Vakhrushev, and E. Suard, Phys. Rev. B **65**, 024104 (2001).
[6] O. Svitelskiy, J. Toulouse, G. Yong, and Z.-G. Ye, Phys. Rev. B **68**, 104107 (2003).
[7] B. Dkhil, P. Gemeiner, A. Al-Barakaty, L. Bellaiche, E. Dulkin, E. Mojaev, and M. Roth, Phys. Rev. B **80**, 064103 (2009).
[8] C. Stock, L. Van Eijck, P. Fouquet, M. Maccarini, P. M. Gehring, G. Xu, H. Luo, X. Zhao, J.-F. Li, and D. Viehland, Phys. Rev. B **81**, 144127 (2010).
[9] S. Prosandeev, I. P. Raevski, M. A. Malitskaya, S. I. Raevskaya, H. Chen, C.-C. Chou, and B. Dkhil, J. Appl. Phys. **114**, 124103 (2013).
[10] V. Westphal, W. Kleemann, and M. D. Glinchuk, Phys. Rev. Lett. **68**, 847 (1992).
[11] E. V. Colla, E. Yu. Koroleva, N. M. Okuneva, and S. B. Vakhrushev, Ferroelectrics **184**, 209 (1996).
[12] R. Pirc, Z. Kutnjak, and N. Novak, J. Appl. Phys. **112**, 114122 (2012).
[13] G. Xu, G. Shirane, J. R. D. Copley, and P. M. Gehring, Phys. Rev. B **69**, 064112 (2004).
[14] H. Takenaka, I. Grinberg, and A. M. Rappe, Phys. Rev. Lett. **110**, 147602 (2013).
[15] I. Grinberg and A. M. Rappe, Phys. Rev. B **70**, 220101(R) (2004).
[16] S. Tinte, B. P. Burton, E. Cockayne, and U. V. Waghmare, Phys. Rev. Lett. **97**, 137601 (2006).
[17] P. Ganesh, E. Cockayne, M. Ahart, R. E. Cohen, B. Burton, R. J. Hemley, Y. Ren, W. Yang, and Z.-G. Ye, Phys. Rev. B **81**, 144102 (2010).
[18] D. Wang, A. A. Bokov, Z.-G. Ye, J. Hlinka, and L. Bellaiche, Nat. Commun. **7**, 11014 (2016).
[19] Y. Nahas, S. Prokhorenko, I. Kornev, and L. Bellaiche, Phys. Rev. Lett. **116**, 127601 (2016).
[20] J. C. Slater, Phys. Rev. **78**, 748 (1950).
[21] B. E. Vugmeister and M. D. Glinchuk, Rev. Mod. Phys. **62**, 993 (1990).
[22] S. Prosandeev, D. Wang, A. R. Akbarzadeh, and L. Bellaiche, J. Phys.: Condens. Matter **27**, 223202 (2015).
[23] F. Chu, N. Setter, and A. K. Tagantsev, J. Appl. Phys. **74**, 5129 (1993).
[24] R. Hemphill, L. Bellaiche, A. Garćia, and D. Vanderbilt, Appl. Phys. Lett. **77**, 3642 (2000).
[25] P. K. Davies and M. A. Akbas, J. Phys. Chem. Solids **61**, 159 (2000); J. Am. Ceram. Soc. **80**, 2933 (1997).
[26] M. A. Akbas and P. K. Davies, J. Am. Ceram. Soc. **83**, 119 (2000).
[27] J. M. Cowley, Phys. Rev. **77**, 669 (1950); **120**, 1648 (1960).
[28] K. A. Mader and A. Zunger, Phys. Rev. B **51**, 10462 (1995).
[29] L. Bellaiche and A. Zunger, Phys. Rev. B **57**, 4425 (1998).
[30] A. M. George, J. Íñiguez, and L. Bellaiche, Phys. Rev. Lett. **91**, 045504 (2003).
[31] A. Al-Barakaty, S. Prosandeev, D. Wang, B. Dkhil, and L. Bellaiche, Phys. Rev. B **91**, 214117 (2015).
[32] See Supplemental Material at http://link.aps.org/supplemental/10.1103/PhysRevB.94.180102 for more details about the effective Hamiltonian used here.
[33] J. Íñiguez and L. Bellaiche, Phys. Rev. B **73**, 144109 (2006).
[34] K. M. Rabe and E. Cokayne, *First-Principles Calculations for Ferroelectrics: Fifth Williamsburg Workshop*, edited by R. E. Cohen (AIP, Woodbury, NY, 1998), p. 61.
[35] S. Prosandeev, D. Wang, and L. Bellaiche, Phys. Rev. Lett. **111**, 247602 (2013).
[36] D. Stauffer and A. Aharony, *Introduction to Percolation Theory* (Taylor and Francis, London, 1994).
[37] V. M. Ishchuk, V. N. Baumer, and V. L. Sobolev, J. Phys.: Condens. Matter **17**, L177 (2005).
[38] N. Takesue, Y. Fujii, M. Ichihara, and H. Chen, Phys. Rev. Lett. **82**, 3709 (1999).
[39] I. P. Swainson, C. Stock, P. M. Gehring, G. Xu, K. Hirota, Y. Qiu, H. Luo, X. Zhao, J.-F. Li, and D. Viehland, Phys. Rev. B **79**, 224301 (2009).
[40] A. M. George, J. Íñiguez, and L. Bellaiche, Phys. Rev. B **65**, 180301(R) (2002).
[41] Note that by symmetry, studying the Fourier transform of the y and z components of the local modes should give results similar to those depicted in Fig. 2(b) but in symmetrically-equivalent planes (e.g., in (100) planes if focusing on the Fourier transform of the y components of the local modes).
[42] These special q points naturally depend on the size of the supercell, e.g., they become $2\pi(n_x,n_y,nz)/16a_{\text{lat}}$, with $(n_x,n_y,nz) = (2,0,-2)$, $(-2,0,2)$, $(-2,2,0)$, $(2,-2,0)$, $(-2,-2,0)$, $(2,2,0)$, $(2,0,2)$, and $(-2,0,-2)$, when investigating $16 \times 16 \times 16$ supercells.
[43] L. Bellaiche, J. Íñiguez, E. Cockayne, and B. P. Burton, Phys. Rev. B **75**, 014111 (2007).
[44] A. R. Akbarzadeh, S. Prosandeev, E. J. Walter, A. Al-Barakaty, and L. Bellaiche, Phys. Rev. Lett. **108**, 257601 (2012).
[45] D. Phelan, C. Stock, J. A. Rodriguez-Rivera, S. Chi, J. Leao, X. Long, Y. Xie, A. A. Bokov, Z.-G. Ye, P. Ganesh, and P. M. Gehring, Proc. Natl. Acad. Sci. USA **111**, 1754 (2014).